Crowdsourced Doppler Measurements of Time Standard Stations Demonstrating Ionospheric Variability

Kristina Collins[1], John Gibbons[1], Nathaniel Frissell[2,4], Aidan Montare[3], David Kazdan[1], Darren Kalmbach[4], David Swartz[4], Robert Benedict[4], Veronica Romanek[2], Rachel Boedicker[1], William Liles[4,6], William Engelke[5], David G. McGaw[7], James Farmer[4], Gary Mikitin[4], Joseph Hobart[4], and George Kavanagh[4]

[1]Case Western Reserve University, Glennan Bldg 9A, 10900 Euclid Avenue, Cleveland Ohio 44106
[2]Department of Physics and Engineering, University of Scranton, Scranton PA
[3]National Institute of Standards and Technology, Boulder CO
[4]HamSCI Community
[5]University of Alabama, Huntsville AL
[7]Department of Physics and Astronomy, Dartmouth College, Hanover NH
[6]Liles Innovations LLC, Reston VA

Correspondence: Kristina Collins (kd8oxt@case.edu)

Abstract. Ionospheric variability due to atmospheric coupling produces measurable effects in Doppler shift of HF (high frequency, 3-30 MHz) skywave signals. These effects are straightforward to measure with low-cost equipment and are conducive to citizen science campaigns. The Personal Space Weather Station network is a modular network of community-maintained, open-source receivers, which measure Doppler shift in the precise carrier signals of time standard stations WWV, WWVH and

5   CHU. Here, data from the first prototype of the Low-Cost Personal Space Weather Station are presented for a period of time spanning late 2019 to early 2022. Software tools for the visualization and analysis of this living dataset are also discussed and provided. These tools are robust to data interruptions and to the addition, removal or modification of stations, allowing both short- and long-term visualization at higher density and faster cadence than other methods. These data are archived at www.doi.org/10.5281/zenodo.6622111 (Collins, 2022).

1 Introduction

HF (high frequency, 3-30 MHz) Doppler sounding is an established means of observing the bottomside ionosphere. Its principle of operation is straightforward: a shift in signal path length effects a corresponding Doppler shift, which can serve as a proxy for change in ionospheric height. This information may be integrated with other ionospheric measurements to examine ionospheric variability resulting from geophysical events.

15   In recent years, enabling technologies have become prevalent which reduce the barriers to performing precise Doppler measurements. In particular, single-board computing greatly reduces the expense and difficulty of datalogging, and readily available GPS-disciplined oscillators (GPSDOs) allow for precision timing at a price point on the order of 100 USD. The price burden for this method is also reduced by the use of existing time standard stations, such as WWV, WWVH and CHU.

These stations broadcast national standard time via AM signals with precisely controlled carriers, providing ideal signals of
20   opportunity.

Accordingly, it is now tenable to create distributed systems of HF Doppler receivers which serve as a "meta-instrument" for
the observation of ionospheric disturbances, either in short term campaigns such as the one recorded in Collins et al. (2022b),
or in long-term data collection such as in the dataset presented herein. Such systems are readily supported by citizen scientists
in the amateur radio and shortwave listening communities (Collins et al., 2021; Frissell et al., 2022b).

25   These data are useful to geospace scientists seeking to build a more complete picture of short term events (lasting hours
to days) which occurred during the recorded timeframe, such as solar flares and geomagnetic storms. Today, frontier science
investigations in these fields generally rely on combining observations from multiple instrument platforms, including total elec-
tron content estimations derived from the Global Navigation Satellite System (GNSS TEC) (Vierinen et al., 2016), incoherent
scatter radar (ISR) (Nicolls and Heinselman, 2007; Zhang et al., 2021), SuperDARN radar (Nishitani et al., 2019), and vertical
30   ionosondes (Hunsucker, 1991; Scotto et al., 2012), among others. Oblique HF sounders such as the ones used in this dataset
represent one of many tools for the multi-instrument observer, and can provide direct benefit to these investigations.

Further insights may also be developed by examination of long-term trends. As discussed in Section 4.3, seasonal variations
are clearly evident in the longest datasets collected at the time of writing. As observations continue throughout Solar Cycle 25,
we expect that these Doppler data, recorded at a greater level of coordination in the long term than has generally been achieved
35   in the past, will support or yield novel analyses of long-term trends in ionospheric variability.

2   Background

Understanding ionospheric variability remains a frontier topic in the space physics community. This variability is key not only
to understanding ionospheric dynamics in its own right, but also as a means to understanding the coupled geospace system
as a whole, which includes the ionosphere's connection to both space above and the neutral atmosphere below. Ionospheric
40   variability takes on many forms and arises from many sources. Some forms are better understood than others. Sources of vari-
ability from space include solar flares that last minutes, *e.g.*, (Dellinger, 1937; Benson, 1964; Chakraborty et al., 2018, 2021);
substorms that last a few hours, *e.g.*, (Gjerloev et al., 2007; Blagoveshchenskii, 2013; Hori et al., 2018); and ionospheric
and geomagnetic storms that can last days, *e.g.*, (Buonsanto, 1999; Prölss, 2008; Thomas et al., 2016). Sources of variability
from below include traveling ionospheric disturbances (TIDs) associated with atmospheric gravity waves (AGWs) *e.g.*, (Hines,
45   1960; Hunsucker, 1982). These may be caused by tornadoes (Nishioka et al., 2013), tsunamis (Galvan et al., 2011; Huba et al.,
2015), or high latitude sources (Grocott et al., 2013; Frissell et al., 2016).

To understand this variability, it is important to measure over both large spatial and temporal domains and with high resolu-
tion. While many large-scale professional ionospheric sensing networks exist, the ionosphere remains significantly undersam-
pled. To help address this undersampling issue, members of the Ham Radio Science Citizen Investigation (HamSCI) collective
50   are working to develop the Personal Space Weather Station (PSWS), a modular, multi-instrument, ground-based space science
observation platform that can be operated and afforded by individuals, as described in Collins et al. (2021, 2022b). The low-
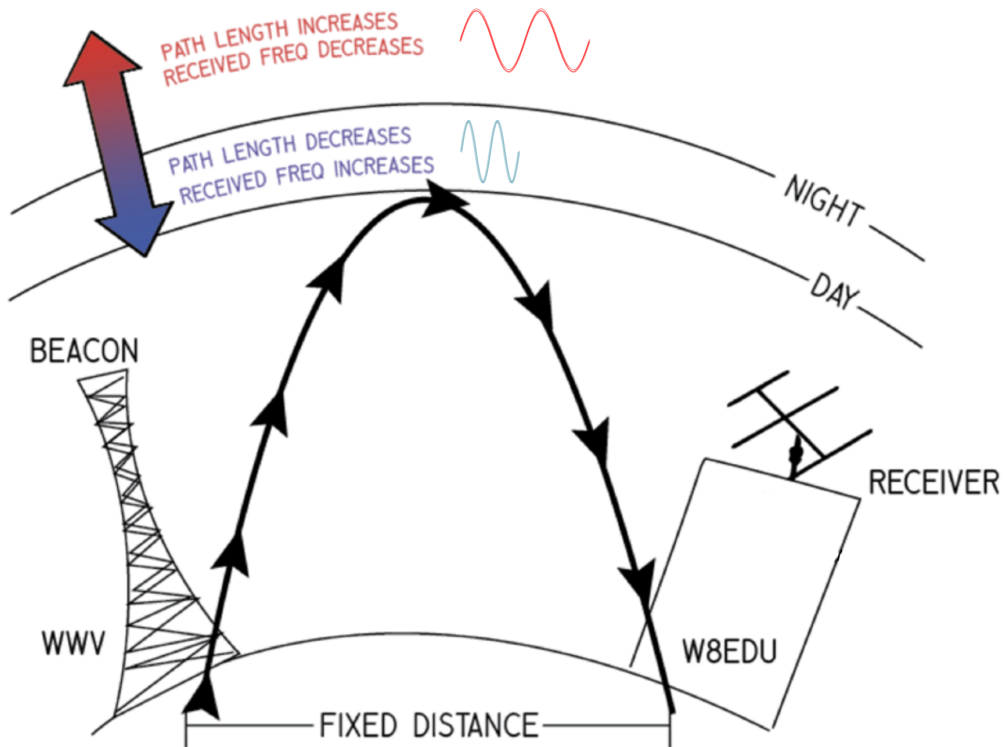
Figure 1. A notional illustration of the relationship between shift in ionospheric layer height and received frequency shift. Precision frequency standards are required at both beacon and receiver in order to make an effective comparison. Frequency variation is generally on the order of ± 1 Hz. Multihop propagation and Pedersen modes are not shown.

cost version of the PSWS is known as the Grape, documented by Gibbons et al. (2022b). The Grape is a precision, narrowband, high frequency (HF) receiver that observes ionospheric variability by measuring the Doppler shift of signals emitted by highly-stable transmitters, such as WWV and WWVH operated by the U.S. National Institute of Standards and Technology (NIST) and CHU operated by the Institute for National Measurement Standards of the National Research Council of Canada.

The Doppler shift mechanism is illustrated in Figure 1. Here, WWV transmits a HF signal that is refracted by the ionosphere back to Earth where it is received by station W8EDU. Ionospheric variability related to peak layer height, peak layer electron density, and/or layer thickness can cause changes in the propagation path that are sensed as positive Doppler shifts for decreasing path lengths (blueshifts) and negative Doppler shifts for increasing path lengths (redshifts) (Lynn, 2009). Assuming the observed Doppler shifts are a function of the rate of change in layer height, Doppler shifts can be used to estimate changes of the relative altitude at the ionospheric refraction point (Collins et al., 2022a). Doppler shift variations can also be used to measure the period, wavelength, and direction of TIDs (Georges, 1968; Crowley and Rodrigues, 2012; Chilcote et al., 2015; Trop et al., 2021; Trop, 2021; Romanek et al., 2022).

3 Methodology

3.1 Hardware

65

The majority of stations in this dataset use the purpose-built Grape V1, a low-cost receiver described by Gibbons et al. (2022b). This is a low intermediate frequency receiver optimized for Doppler measurements.

It is also possible to use the software components with other hardware: as noted in the `nodelist.csv` file in the software repository, which is included in abridged form in Table A1, some of the registered nodes collect data using commercial off-the-

70 shelf (COTS) amateur radio receivers which are capable of accepting an external frequency input from, *e.g.*, GPS-disciplined oscillators. Citizen scientists from the amateur radio and shortwave listening communities can therefore leverage their existing hardware to contribute to the PSWS network at no additional cost, and with no licensure requirement. The data processing framework of the Personal Space Weather Station network is robust to the addition and modification of new nodes, as well as to data outages. Data collected up to 1 June 2022 are represented in the data inventory shown in Figure 5.

75 ### 3.2 Data acquisition process

The process of data curation is depicted in Figure 2. Each station collects 24-hour datasets according to an established standard and uploads them on a daily basis to a central FTP server. The data are then manually cleaned to eliminate test files, corrupted files and spurious uploads, and consolidated into a single .zip file, which is posted to the data repository at (Collins, 2022). While the size of the final .zip file varies according to the number of stations collecting data, the efficiency of compression, and

80 other factors, it is on the order of a few GB. The updated dataset can then be downloaded from Zenodo to a subdirectory in the code repository at (Frissell et al., 2022a), and used to create updated versions of the visualizations discussed in this paper.

3.3 File Format and Description

An example file is shown in Figure 3, which shows a file with corresponding filename `2020-07-09T000000Z_N0000001` `_G1_EN91fh_FRQ_WWV10.csv`. This filename includes, in order: the date the data was collected and the time at which that

85 collection began; the node number, corresponding to the list in Table A1; the type of radio being used (*e.g.*, "G1" indicates a Grape Version 1); the Maidenhead grid square in which the data was recorded; and the time standard station being measured. A detailed description of the file format and upload process is available at Collins (2021). Metadata at the beginning of each file records station information, including room for comments. The main table has three columns: UTC time, estimated frequency, and received power.

90 ## 4 Data Visualization

The visualization code in Frissell et al. (2022a) allows for the dynamic visualization of station availability and datasets. Results can be examined in the short- or long-term, for one station in isolation or in comparison to others. Examples of this visualization code are given below. Section 4.1 describes the map and Gantt chart which summarize where and when station data is
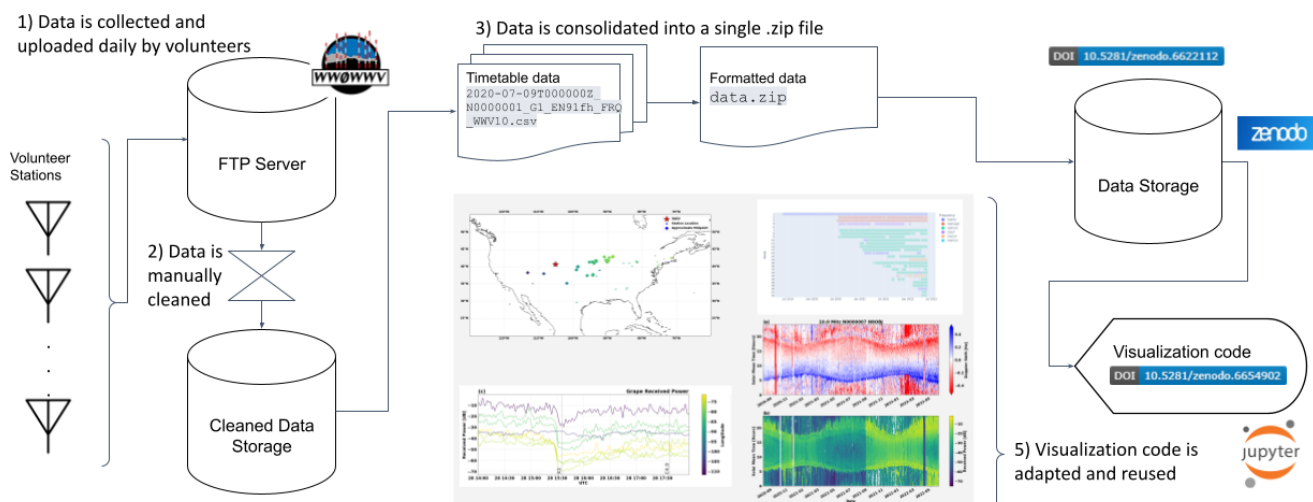
Figure 2. A graphical abstract showing how the data are collected, as described in Section 3.2. The visualization figures are rendered at full scale elsewhere in this paper.

available for a given period of time. Sections 4.2 and 4.3, respectively demonstrate short- and long-term analyses of data from
95 a single station. Subsequent sections focus on the detection of geophysical signatures: Section 4.4 demonstrates the detection
of signatures consistent with traveling ionospheric disturbances, while Section 4.5 showcases the detection of solar flares by
multiple Grape stations.

4.1 Station Availability

A map of stations to date is shown in Figure 4. Stations were chosen on a volunteer basis, with some specifically recruited to
100 improve coverage. Clusters of stations are evident around universities involved in the project: Case Western Reserve University
in Cleveland, University of Scranton in Pennsylvania, and the New Jersey Institute of Technology each have a collection of
nodes belonging to researchers. An additional cluster is generated by volunteers of the New England amateur radio community.
In some cases, maintainers were recruited specifically to provide coverage in areas of interest, such as Node 18 in California.
There are also nodes close to WWV in the Fort Collins, Colorado area (*e.g.*, Node 13) which are within the transmitter's radio
105 horizon and can be used to confirm that trends in the data originate with the ionosphere and not the radio transmitters.

Several stations are registered as nodes but do not have data included in the dataset reported at the time of writing. This may
be for one of three reasons: first, the station may have data recorded but not uploaded to the FTP server; second, the station
may be in the process of installing a node; third, the station may be used for experimentation with new data collection methods,
including spectrum sampling and other frequency analysis algorithms. A central aspect of this work is its architecture as a
110 living dataset, *i.e.*, a dataset into which new stations and historic data may be easily incorporated.

```
#,2020-07-09T00:00:00Z,N0000001,EN91fh,41.3219273, -81.5047731, 285,Macedonia Ohio,G1,WWV10
####################################
# MetaData for Grape Gen 1 Station
#
# Station Node Number      N0000001
# Callsign                 N8OBJ
# Grid Square              EN91fh
# Lat, Long, Elv           41.3219273, -81.5047731, 285
# City State               Macedonia Ohio
# Radio1                   Grape Gen 1 Rcvr 1
# Radio1ID                 G1
# Antenna                  135 Foot OCF Dipole 30 Feet up
# Frequency Standard       LB GPSDO
# System Info              RasPi4B w/4GB, Raspian OS, FLDigi V4.1.13 (N8OBJ Modified)
#
# Beacon Now Decoded       WWV10
#
####################################
# --- Extra Metadata File ---
# Metadata Line #1
# Metadata.txt file contains no real info 8-{
# Special Chars are allowed !@#$%^&*()_-+={}[]|\:':"<>?,/.
# This is the last line - 73
#
UTC,Freq,Vpk
2020-07-10T00:00:00Z, 10000000.344, 0.000001
2020-07-10T00:00:01Z, 10000000.179, 0.000001
2020-07-10T00:00:02Z, 10000000.896, 0.000001
2020-07-10T00:00:03Z, 10000000.952, 0.000001
2020-07-10T00:00:04Z, 10000000.067, 0.000001
2020-07-10T00:00:05Z, 10000000.428, 0.000001
2020-07-10T00:00:06Z, 10000000.085, 0.000001
2020-07-10T00:00:07Z, 10000000.701, 0.000001
2020-07-10T00:00:08Z, 10000000.537, 0.000001
2020-07-10T00:00:09Z,  9999999.700, 0.000001
pi@PSWSGrape1:/home/pi/PSWS/Sdata$
```

Figure 3. An example of a one-day data file with integrated metadata. This file will have the filename `2020-07-09T000000Z_N0000001_G1_EN91fh_FRQ_WWV10.csv`. The file contents are self-documenting.

Figure 5 shows the data collected by each node over time. The network is modular: new stations can easily be added, and data analysis procedures are tolerant of outages and changes in frequency for each node.

4.2 Sunrise and Sunset

The plotting routine automatically computes the local sunrise and sunset for a given station location, and shades the background
115 accordingly. An example of data collected by Node 1 during the Festival of Frequency Measurement campaign recorded in Collins et al. (2022b) is shown in Figure 6. The output produces two plots: Doppler shift on the top and amplitude on the bottom. In each case, the raw data, scatter-plotted in blue, undergoes filtering to produce the filtered result, which is overlaid in
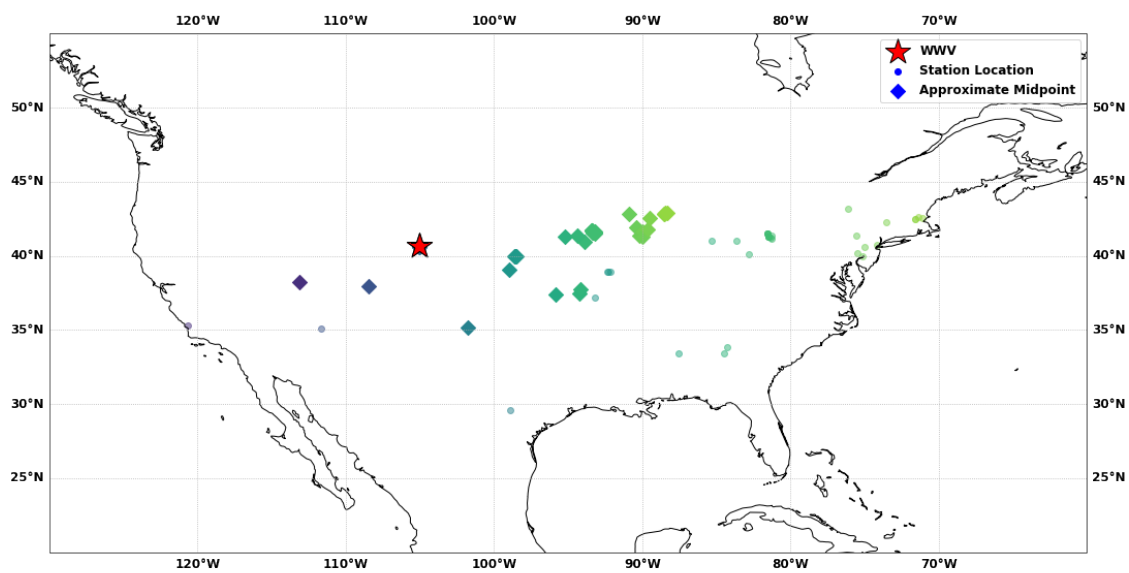
Figure 4. A map of currently deployed Grape stations in the United States. Per Table A1, some international stations are not shown. Scatter points mark the locations of each station, and diamonds mark the approximate geographical midpoint between each station and WWV. Each pair of points are color-coded by station longitude.
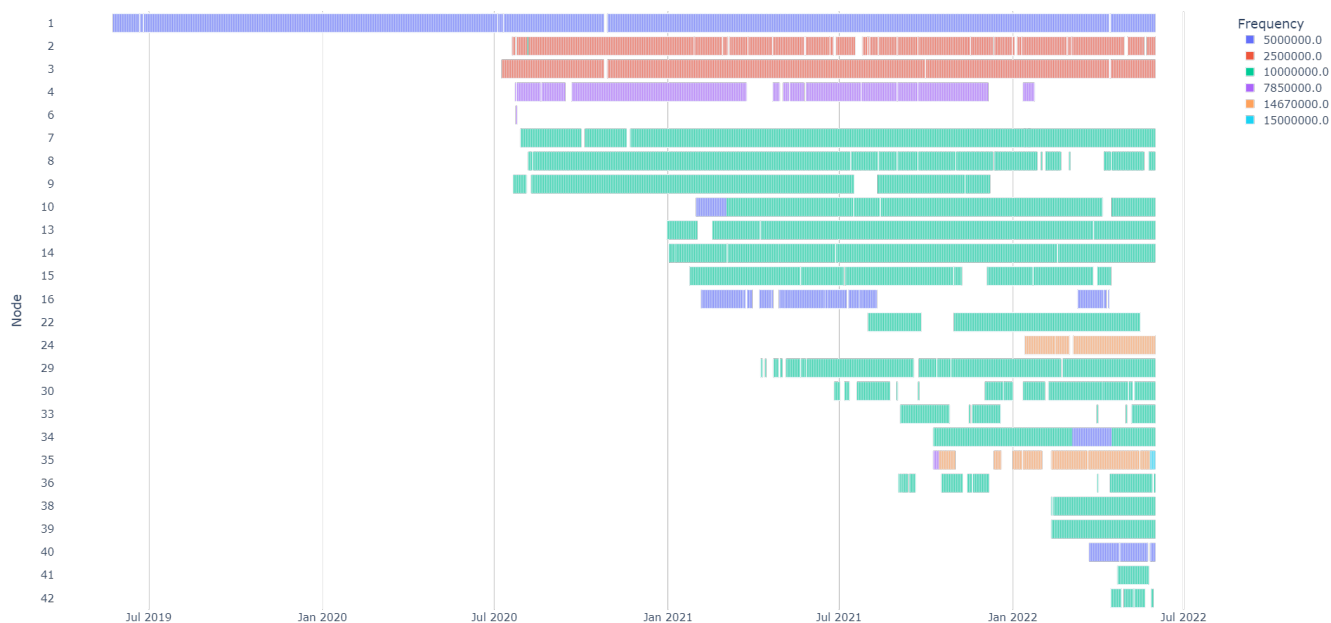
Figure 5. A data inventory, produced with a Gantt plotting tool in plotly express (Inc., 2015), showing the data collected by each node.

yellow. By default, the data processing uses a Butterworth low-pass filter with parameters plotted in Figure 7. A similar plotting routine is used to provide station maintainers with daily feedback, as described and depicted in Figures 10 – 13 of (Gibbons

120 et al., 2022b). Sunrise and sunset fluctuations vary with local conditions but are distinct in long-term data, as discussed in Section 4.3.

4.3 Long-Term Climatology

Long-term trends in the data of Node 7 are shown in the time-date-parameter plots of Figure 8. Two plots are shown: Doppler shift in Hertz using a red/blue divergent colormap (*cf.* Appendix B) and received power in decibels. Each day represents a

125 line of pixels from bottom to top, with corresponding solar mean time lined up across the plots horizontally. On the horizontal axis, time's arrow runs left to right, covering a span from mid-2020 to spring 2022. Several observations, both geophysical and instrumentation-related in nature, can be gleaned from these two plots. First, the seasonal movement of sunrise and sunset is clearly visible at the bottom and top of the frequency plot respectively. The amplitude plot on the bottom demonstrates that reception from WWV to this station's location in the Cleveland area is much better during the nighttime, when the F2 layer

130 of the ionosphere allows a propagation path to open up between the two locations; therefore, the signals above the sunrise line (*i.e.*, nighttime) on the frequency plot may be associated with geophysical variation, while the signals on the bottom are likely only noise. Vertical stripes toward the left side of both plots indicate changes or gaps in instrumentation, which are
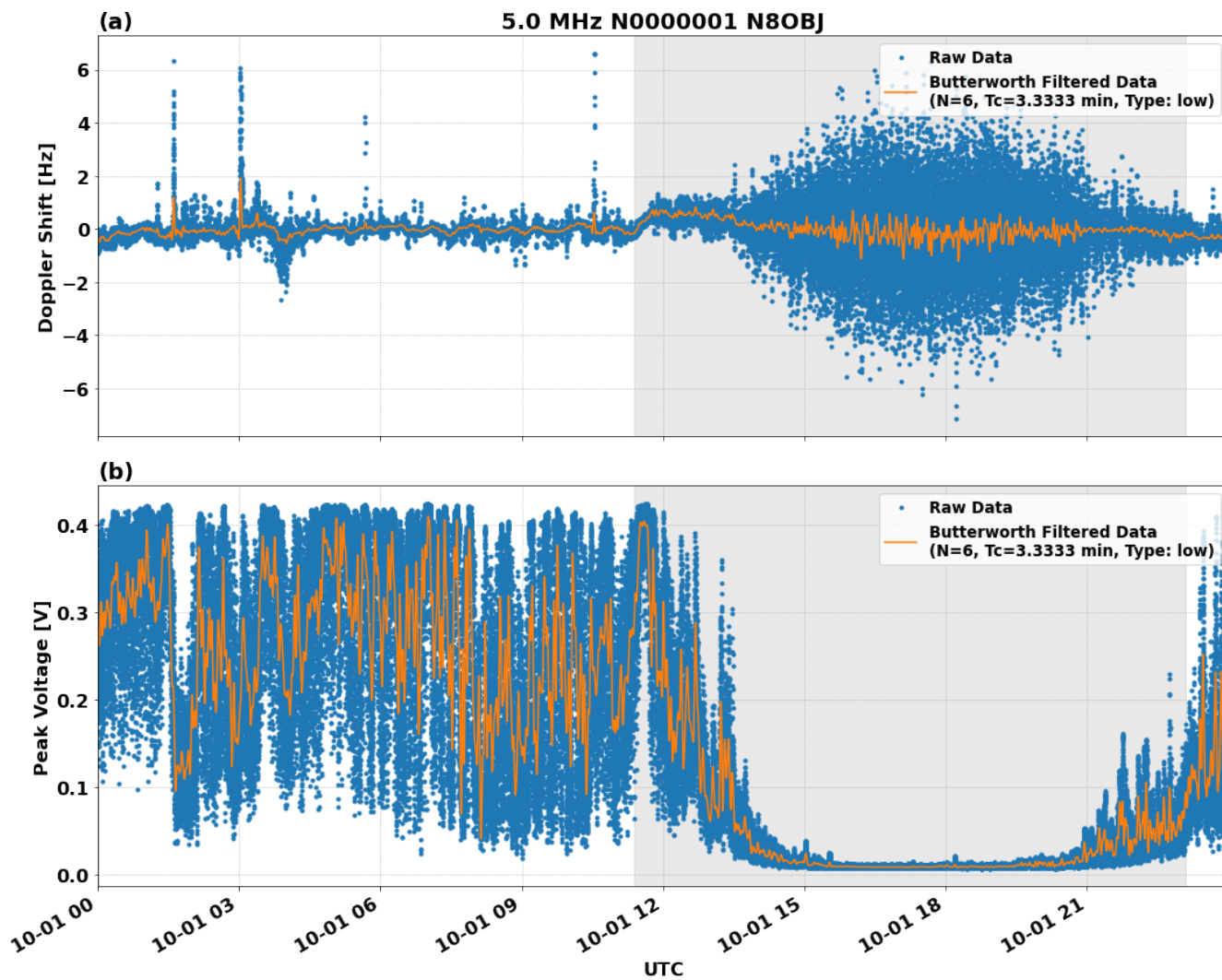
Figure 6. Frequency and amplitude plots of Node 1's data from 1 October 2019, with sunrise and sunset indicated by background shading. The result of the standardized processing chain using the filter in Figure 7 is superimposed on the raw data. The sunrise peak described in Gibbons et al. (2022b) is clearly visible.
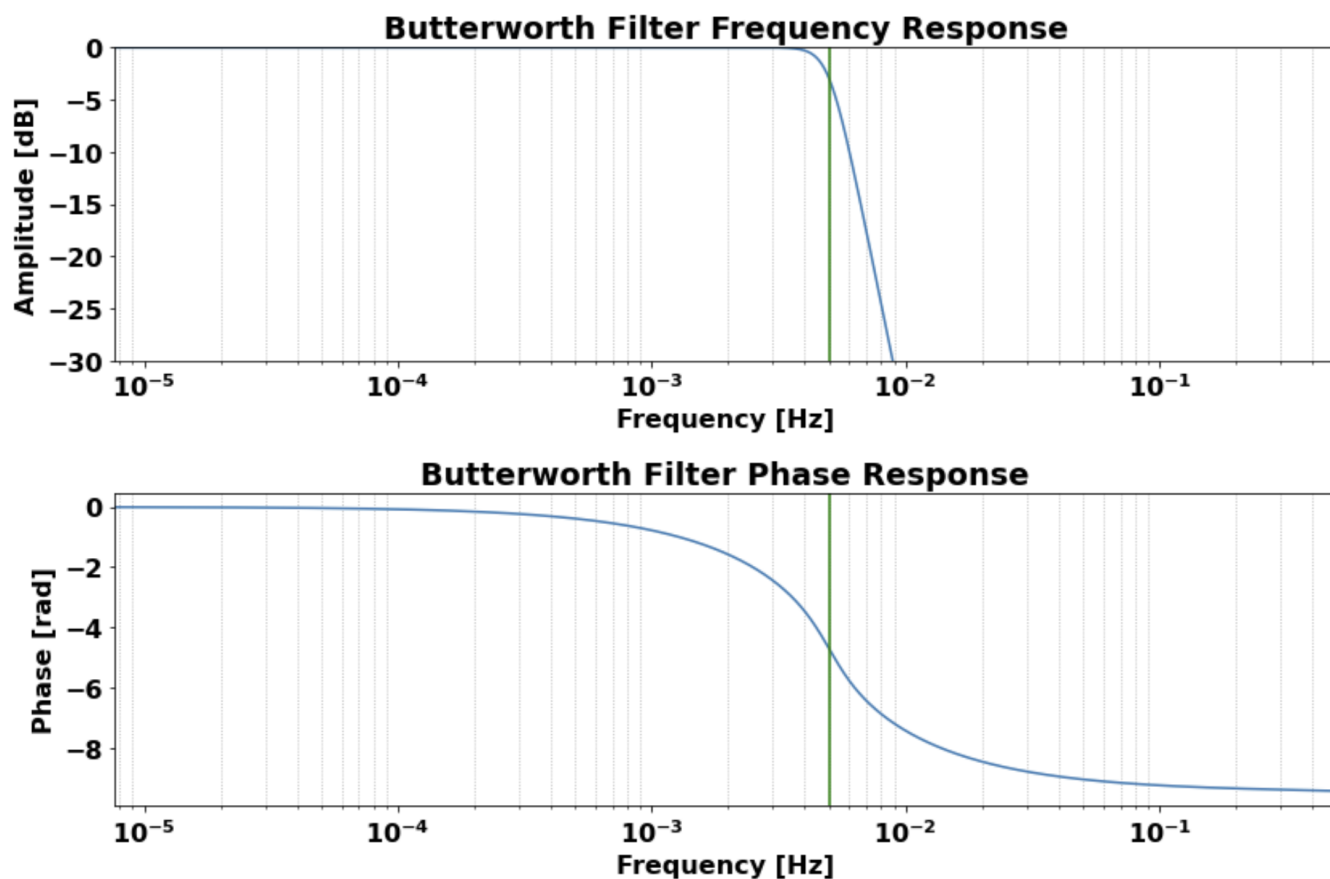
Figure 7. Frequency response characteristics of the Butterworth low-pass filter used to produce Figure 6.

also reflected in the metadata for the affected time period. In this station's case, the station maintainer recorded a change of antenna at his station on 26 August 2021, when he switched from an off-center-fed dipole to a magnetic loop antenna with a

135   preamplifier. This change produced an overall increase of received power, which is clearly visible in the power plot. The lack of a corresponding change in the frequency plot above it indicates that the frequency estimation algorithm was able to function well with either antenna.

4.4   Traveling Ionospheric Disturbances

One category of ionospheric phenomena of particular note are medium-scale traveling ionospheric disturbances (MSTIDs), de-

140   fined by Hunsucker (1982) as wavelike perturbations of ionospheric plasma with wavelengths of hundreds of kilometers, phase velocities of hundreds of meters per second and periods between 10 minutes and 1 hour. While MSTIDs may be associated with either atmospheric gravity waves (AGWs) from the neutral atmosphere (e.g., Hines, 1960; Bristow et al., 1994; Frissell
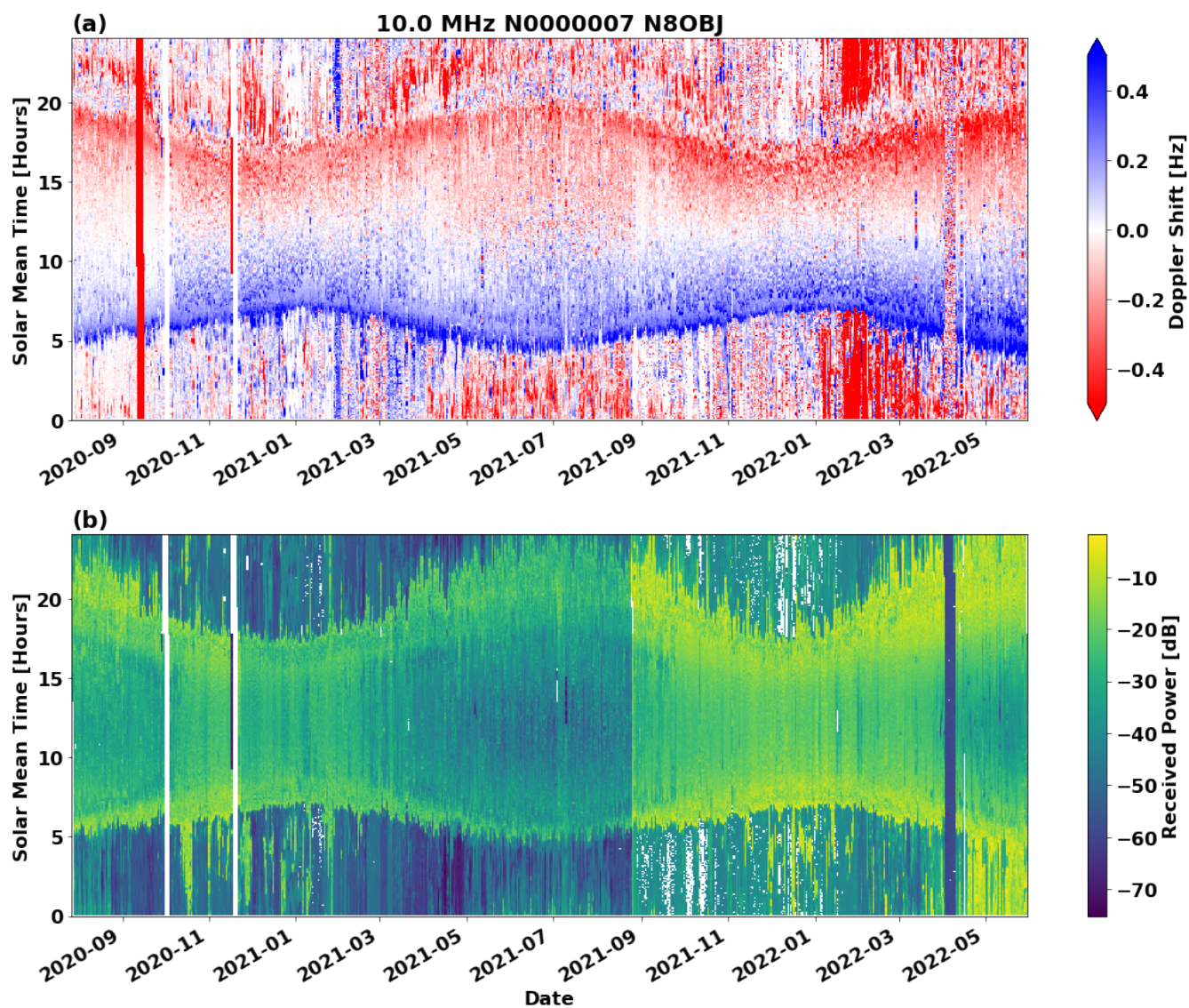
Figure 8. Heatmaps of frequency (top) and amplitude (bottom) at Node 1. Each day represents a line of pixels from top to bottom, with corresponding UTC times lined up across the plots horizontally. The seasonal movement of sunrise and sunset is clearly visible in both plots.

Earth System
Open Access · Science
Data
Discussions
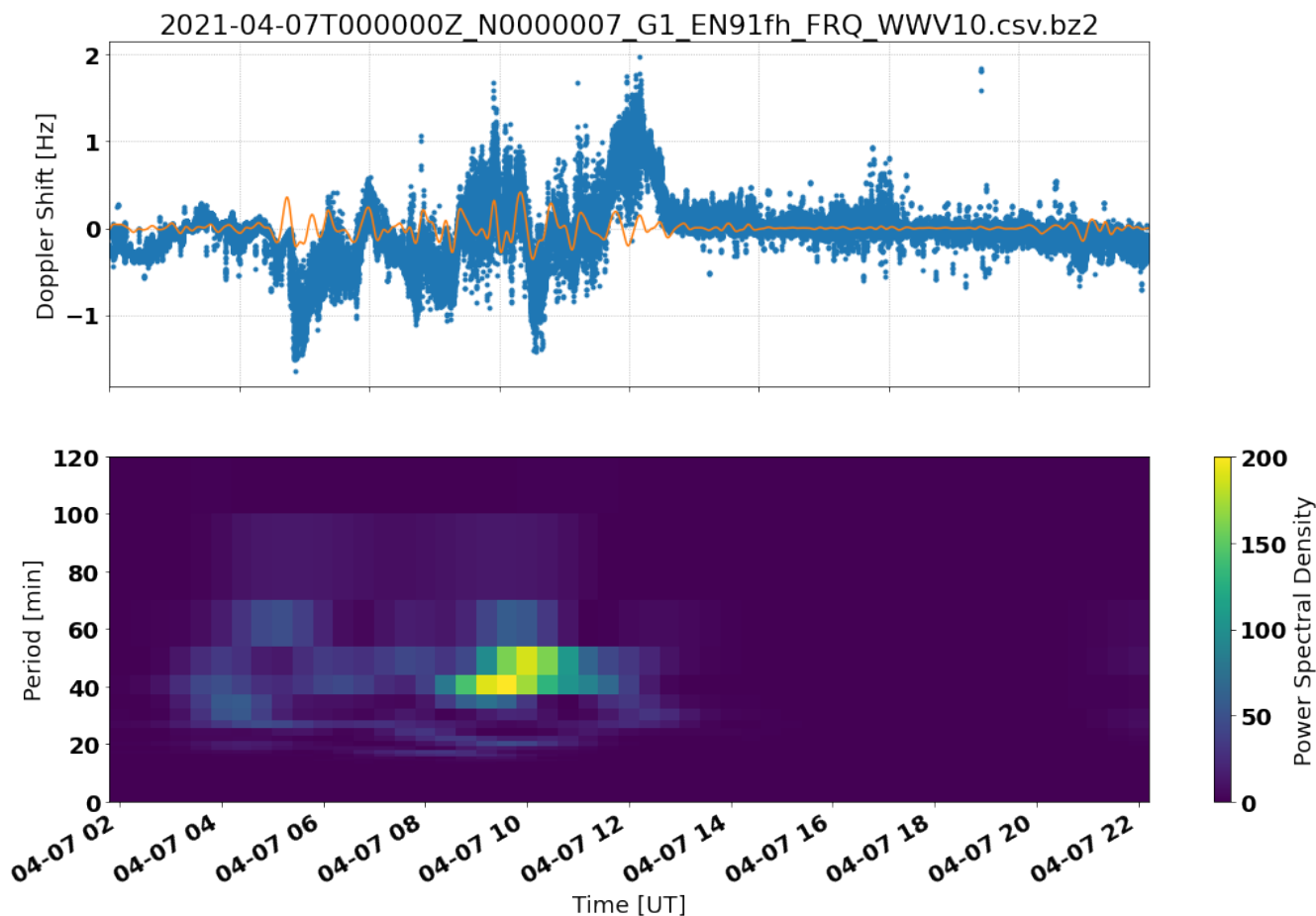
Figure 9. Power spectral density plot showing signatures consistent with traveling ionospheric disturbances.

et al., 2016) or from electrodynamic processes (e.g., Kelley, 2011; Atilaw et al., 2021), the source of MSTIDs is still not well
understood due to their ubiquitous nature and the complexities of atmosphere-ionosphere coupling.

145   Trop et al. (2021) and Trop (2021) developed a technique to estimate TID period, speed, propagation direction, and velocity
from a network of AM broadcast band Doppler receivers described by Chilcote et al. (2015); this technique is now being
developed for use with HF Grape Doppler data by Romanek et al. (2022). Based on previous work of Georges (1968); Crowley
and Rodrigues (2012); Chilcote et al. (2015); Trop (2021) and Romanek et al. (2022).

Figure 9a is generated using the same standard processing as Figure 6, *i.e.*, the low-pass filter shown in Figure 7. Next, the
150   data is interpolated and filtered with the band-pass filter shown in Figure 10, using a 0.5–1.2 mHz (T = 14–33 min) passband to
isolate the dominant MSTID, similar to the approach used in Sect. 3.1.2 of Frissell et al. (2014). The output is then separated
into four-hour bins with a ninety-percent overlap, and plotted as a spectrogram in Figure 9b, which shows signatures consistent
with MSTIDs.
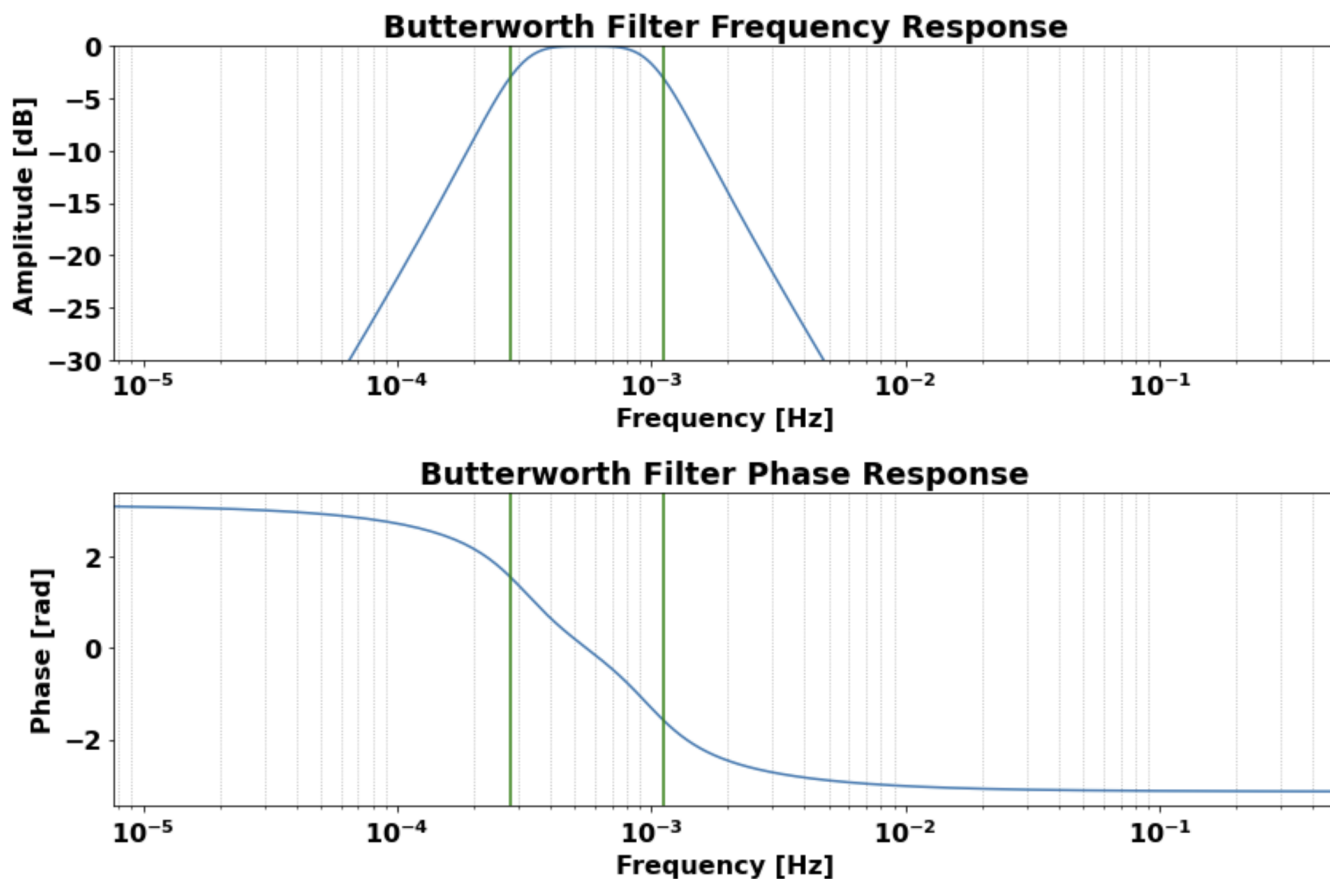
Figure 10. Butterworth filter used in production of Figure 9.

4.5 Ionospheric Response to Solar Flares

155 Figure 11 shows the response of the Grape network to solar flares on 28 October 2021, providing an example of a multi-instrument measurement. The top plot gives the X-ray irradiance as measured by NOAA's GOES-17 spacecraft, with two flares marked: an X-class solar flare with a maximum at 15:35 UTC, and a smaller, C-class flare about two hours later. Figure 11b shows the Doppler shift for eight stations from the day in question, colormapped by station longitude; below it, Figure 11c shows the relative received power for the same stations. A longitude-dependent Doppler flash (Chakraborty et al., 2021)

160 is observed in the frequency plot in conjunction with each flare, and a radio blackout following the X1 flare is observed in the power plot. (The lone exception, Node 13 (W3LLA) is the groundwave station near WWV.)

By default, no scaling is applied in the received power plot of Figure 11c. As discussed in Section 4.3, received signal strength varies with the antenna but may not impact the accuracy of the estimated frequency. Additionally, the PSWS nodes which use commercial off-the-shelf (COTS) hardware rather than Grape receivers (*cf.* Table A1) may have an automatic gain

165 control (AGC) which impacts the utility of the power measurement. Therefore, users are encouraged to begin by examining the
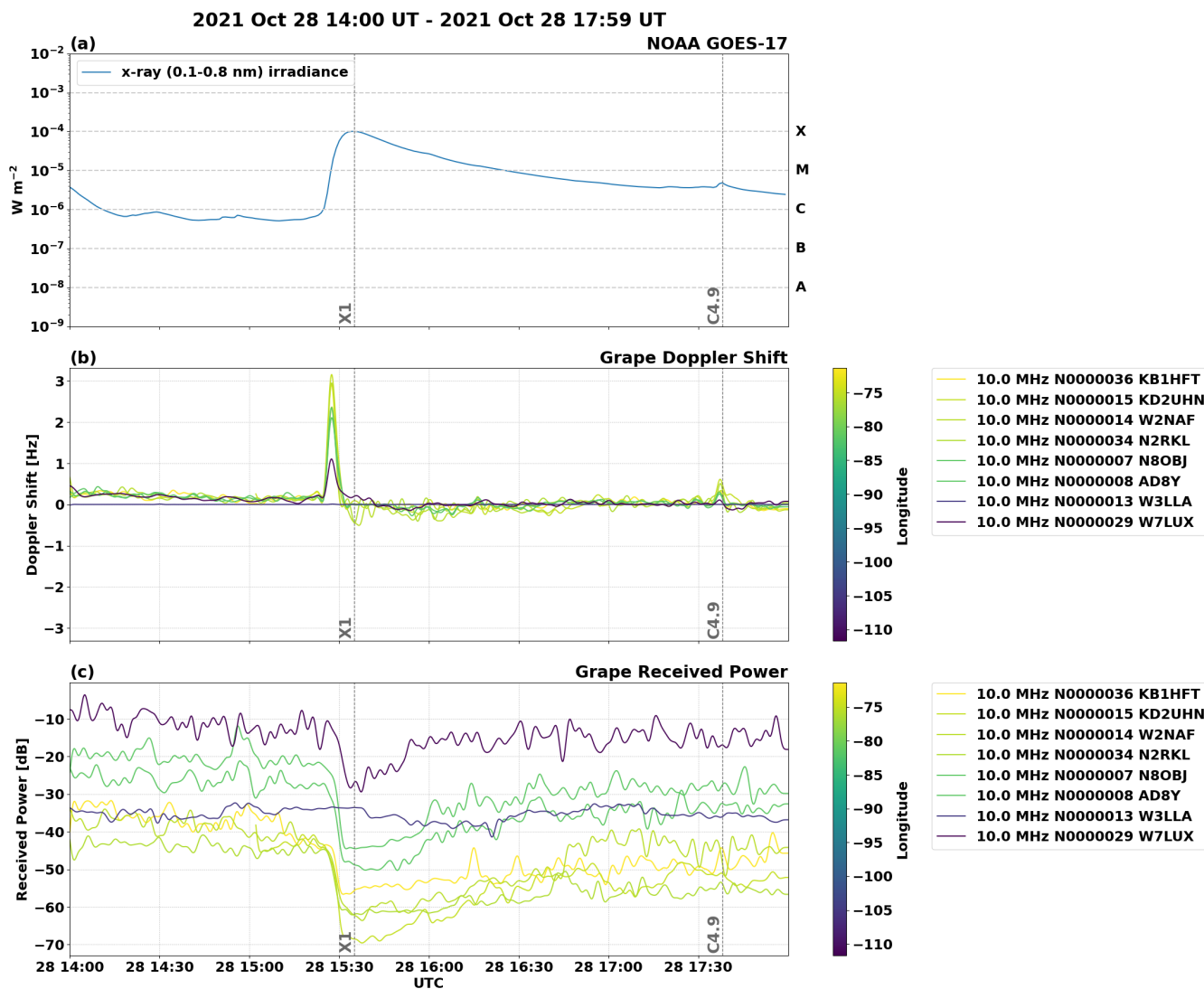
Data

Figure 11. Annotated frequency and amplitude plots showing the response of Grape stations to an X1 solar flare on 28 October 2021.

raw data from an event of interest before applying scaling. A discussion on validation may be found in Section 7 of Gibbons et al. (2022a).

5 Conclusions

1. **We present a living dataset of HF Doppler measurements made by citizen scientists.** These measurements are conducted using time standard stations' carrier signals as precise HF beacons. The amplitude and estimated Doppler shift

170

are recorded at approximately a 1 second cadence by each station. Outages and nonstandard start times are automatically handled within the file format.

2. **A modular framework is presented for the visualization and analysis of these data.** Per Section 6, the code used to prepare the figures in this manuscript is made available for the reader's use. This code may be used to visualize future versions of the dataset as well. Additional nodes may be added to the primary dataset by coordination with the authors.

3. **Doppler data reveal both short- and long-term trends in ionospheric variability.** Exemplars include Figures 8 and 11 above. These data may be used in conjunction with other measurements to address frontier questions in geospace science using a multi-instrument approach.

6 Code and data availability

The figures in this paper were produced using python code and Jupyter notebooks available at `https://github.com/HamSCI/hamsci_psws` (Frissell et al., 2022a). The data are available at `www.doi.org/10.5281/zenodo.6622111` (Collins, 2022). The Grape V1 hardware is fully documented in Gibbons et al. (2022b), and the files to reproduce that hardware are available at Collins (2021).

Appendix A: Table of Grape Stations

Registered nodes at the time of writing are listed in Table A1.

Appendix B: Supplemental Colormaps

The red/blue colormap used for the frequency plot in Figure 8 is not colorblind-compliant. This colormap (`bwr_r` from Gao et al. (2015)) was chosen because it conceptually relates red and blue to red shift and blue shift, and because as a divergent colormap (saturation is lowest at times of minimal change in virtual layer height and highest at times of maximal change) it is well-suited to the data. Finding a divergent colormap which is colorblind-compliant, however, is extremely difficult, and it is not possible to ensure that it will universally meet the needs of all colorblind readers. Therefore, to improve accessibility for these plots, we have included explicit lines in the code for setting the colormap using matplotlib's colormap functions. We encourage the reader to review matplotlib's documentation at `https://matplotlib.org/stable/tutorials/colors/colormaps.html` to find an effective colormap for their needs, and to change the `bwr_r` colormap for another as required. A version of the Doppler heatmap using the viridis colormap is shown in Figure B1.

Additionally, the Colormoves interface described by Samsel et al. (2018) and available at `sciviscolor.org` allows for real-time construction and modification of colormaps using a drag-and-drop interface.
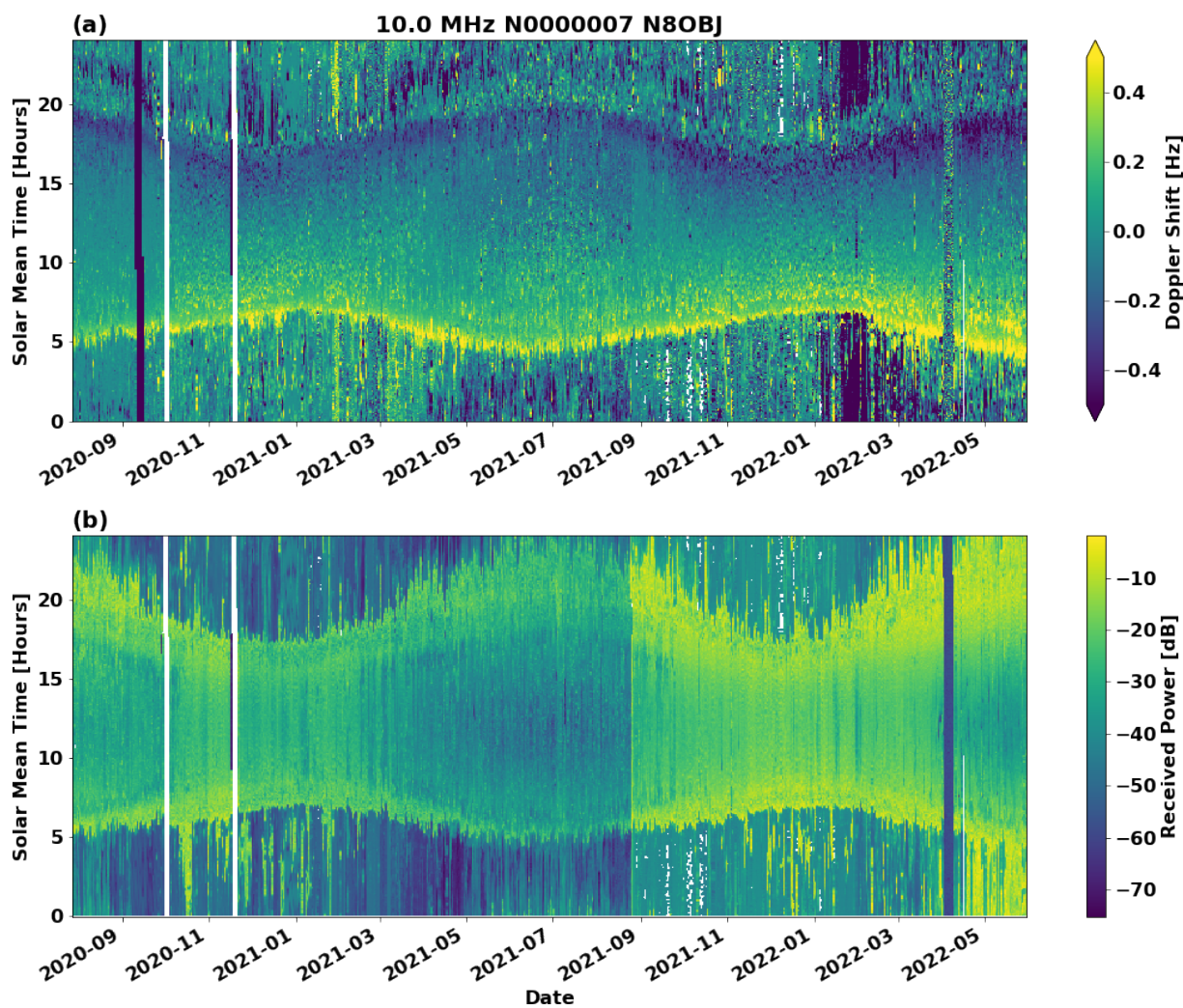
Figure B1. A version of Figure 8 using the perceptually uniform viridis colormap.

Node	Callsign	Name	Grid Square	Latitude	Longitude	Elev. (m)	Radio	Antenna	System
1	N8OBJ	John C. Gibbons	EN91fh	41.32	-81.50	285	Grape Gen 1	DX Eng RF-PRO-1B Mag Loop /w N8OBJ preamp	Raspi3B+, FLDigi 4.1.13
2	AD8Y	David Kazdan	EN91fl	41.49	-81.57	300	ICOM IC-7610	nan	RaspI3B+, FLDigi 4.1.13
3	N8OBJ	John C. Gibbons	EN91fh	41.32	-81.50	285	Grape Gen 1	DX Eng RF-PRO-1B Mag Loop /w N8OBJ preamp	RaspI3B+, FLDigi 4.1.13
4	AD8Y	David Kazdan	EN91fl	41.49	-81.57	300	Grape Gen 1	nan	RaspI3B+, FLDigi 4.1.13
5	KE8HPA	Frankie Bonte	EN80nd	40.13	-82.84	275	DXF1200	nan	RaspI3B+, FLDigi 4.1.09
6	KD8OXT	Kristina Collins	EN91fl	41.49	-81.57	300	DXF1200	nan	RaspI3B+, FLDigi 4.1.09
7	N8OBJ	John C. Gibbons	EN91fh	41.32	-81.50	285	Grape Gen 1	DX Eng RF-PRO-1B Mag Loop /w N8OBJ preamp	RaspI3B+, FLDigi 4.1.13
8	AD8Y	David Kazdan	EN91fl	41.49	-81.57	300	Grape Gen 1	nan	RaspI3B+, FLDigi 4.1.13
9	KB3UMD	Aidan Montare	FN20ge	40.17	-75.49	75	Grape Gen 1	nan	RaspI4B, FLDigi 4.1.13
10	KD8SYG	James Niemann	EN91ii	41.35	-81.28	330	Grape Gen 1	G5RV 80M 102' long	RaspI4B, FLDigi 4.1.13
11	N8OBJ	John C. Gibbons	nan	0.00	0.00	0	Grape Gen 1	nan	RaspI4B, FLDigi 4.1.13
12	WA5FRF	Steve Cerwin	EL09nn	29.57	-98.88	412	ICOM IC-7610 and R8600	30m, 40m, and 160m dipoles	Spectrum Lab, FLDIGI 4.1.14
13	W3LLA	Maxwell Moran	DL70ln	40.54	-105.04	1511	Yaesu FT-817 wLBGPSDO	Wire	RaspI4B, FLDigi 4.1.13
14	W2NAF	Nathaniel A Frissell	FN21ei	41.33	-75.60	0	Grape Gen 1	nan	RaspI4B, FLDigi 4.1.13
15	KD2UHN	Veronica Romanek	FN20mp	40.63	-74.98	136	Grape Gen 1	80M OCF Dipole	RaspI4B, FLDigi 4.1.13
16	WW0WWV	David A Swartz	DN70kn	40.56	-105.11	1546	Grape Gen 1	20M Vertical	RaspI4B, FLDigi 4.1.13
17	WA2UAR	Jay Silber	FM29jw	39.95	-75.17	3	Grape Gen 1	HD6-160 Screwdriver	RaspI4B, FLDigi 4.1.13
18	W6BHZ	Ethan Yoshio Kita [Cal Poly]	CM95qh	35.30	-120.66	0	Grape Gen 1	nan	RaspI4B, FLDigi 4.1.13
19	AB4EJ	Bill Engelke	EM63fj	33.39	-87.54	110	Grape Gen 1	Hexbeam ? 80m dipole	RaspI4B, FLDigi 4.1.13
20	K2MFF	Gareth Perry	FN20vr	40.74	-74.17	50	Grape Gen 1	Inverted V	RaspI4B, FLDigi 4.1.13
21	KV0S	Dave Larsen	EM38tv	38.89	-92.35	220	nan	nan	nan
22	KD8CGH	Robert Benedict	EN91he	41.19	-81.33	300	Grape Gen 1	tuned small loop	RaspI4B, FLDigi 4.1.13
23	KD0EAG	Dave Witten	EM38uw	38.92	-92.29	220	$No_{Radio}1$	$No_{Antenna}$	RaspI-4, 5.4.51-v7l+
24	PA0SLT	Drs. Wim Apon	JO33kg	53.28	6.90	0	Grape Gen 1	nan	RaspI4B, FLDigi 4.1.13
25	K2KGJ	Julius Madey	FN32fg	42.26	-73.54	372	nan	nan	nan
26	KE8QEP	David A. Waugh	EN91id	41.15	-81.25	334	Grape Gen 1	Tuned Horz Dipole 10? Above gnd	RaspI4B, FLDigi 4.1.13
27	W0DAS	David A Swartz	DN70kn	40.56	-105.10	1546	Grape Gen 1	30M Dipole	RaspI4B, FLDigi 4.1.13
28	N1JBJ	William P N Smith	FN42kn	42.56	-71.09	31	Grape Gen 1	40M Homebrew Dipole	RaspI4B, FLDigi 4.1.13
29	W7LUX	Joseph R Hobart	DM45dc	35.09	-111.69	2091	nan	nan	nan
30	K4BSE	Jim Farmer	EM73sj	33.39	-84.47	240	Grape Gen 1 Rcvr 1	Loop	RaspI4B, FLDigi 4.1.13
31	W1MTI	Vladimir A Goncharov	FN42fl	42.49	-71.58	100	Grape Gen 1 Rcvr 1	long wire	RaspI4B, FLDigi 4.1.13
32	AD0RR	Todd Christell	EM37je	37.18	-93.23	382	nan	30 meter dipole	nan
33	AB1XB	Bill Blackwell	FN42el	42.49	-71.59	137	Grape Gen 1 Rcvr 1	30M dipole	RaspI4B, FLDigi V4.1.13
34	N2RKL	Bill Owens	FN13wd	43.16	-76.12	120	Grape Gen 1 Rcvr 1	magnetic loop	RaspI4B, FLDigi V4.1.13
35	PA0RWT	Robert Wagenvoort	JO33lg	53.25	6.95	-2	Flex 1500	Active E-field probe; MiniWhip	RaspI3B+, Fldigi 4.1.13
36	KB1HFT	George Kavanagh	FN42hp	42.63	-71.38	150	Grape Gen 1 Rcvr 1	40m Inverted Vee	RaspI4B, Raspbian OS, FLDigi V4.1.13
37	N8OBJ	John C. Gibbons	EN91fh	41.32	-81.50	285	Grape Gen 2	DX Eng RF-PRO-1B Mag Loop /w N8OBJ preamp	RaspI4B
38	WC0Y	Edward Hall (Ward)	EN71ia	41.019	-85.29	237	Grape Gen 1 Rcvr 1	EWE Wire	RaspI4B, Raspbian OS, FLDigi V4.1.13
39	KM4YMI	Beau Bruce	EM73ut	33.83	-84.28	316	Grape Gen 1 Rcvr 1	tuned loop	RaspI3B+, Raspian OS, FLDigi V4.1.13
40	AC0G	Michael James Hauan	EM38ww	38.91	-92.12	264	OpenHPSDR	wire antenna	RaspI3B+, Raspian OS, FLDigi V4.1.13
41	N8ET	Bill Kelsey	EN80ex	40.99	-83.65	243	Grape Gen 1 Rcvr 1	30m vertical	RaspI4B, Raspbian OS, FLDigi V4.1.13

Table A1. Table of registered nodes at the time of writing.

Author contributions. **Kristina Collins:** Conceptualization, Software, Data Curation, Writing - Original Draft, Investigation, Formal Analysis, Visualization, Project administration. **John Gibbons:** Hardware, Software, Methodology, Investigation, Resources, Project administration. **Nathaniel Frissell:** Conceptualization, Software, Visualization, Formal Analysis, Investigation, Supervision, Funding acquisition, Writing - Original Draft. **Aidan Montare:** Software, Methodology, Investigation. **David Kazdan:** Conceptualization, Methodology, Investigation. **Darren Kalmbach:** Software, Data Curation, Resources. **David Swartz:** Project administration, Investigation. **Robert Benedict:** Investigation, Software, Visualization. **Veronica Romanek:** Investigation, Formal Analysis. **Rachel Boedicker:** Investigation. **William Liles:** Investigation, Formal Analysis. **William Engelke:** Software, Writing - Revision. **David G. McGaw:** Writing - Review & Editing. **James Farmer:** Validation, Investigation, Writing - Review & Editing. **Gary Mikitin:** Validation, Investigation, Writing - Review & Editing. **Joe Hobart:** Validation, Investigation, Writing - Review & Editing. **George Kavanagh:** Investigation, Writing - Review & Editing.

Nota bene: This work was undertaken through the Amateur Radio Science Citizen Investigation (www.hamsci.org). Where possible, amateur radio callsigns are used herein, in addition to names, in order to specify individuals and club stations. Because these callsigns

are unique and persistent identifiers, they support the Findability criterion of FAIR Data principles. The authors' callsigns are KD8OXT,
210 N8OBJ, W2NAF, KB3UMD, AD8Y, KC0ZIE, W0DAS, KD8CGH, KD2UHN, AC8XY, NQ6Z, AB4EJ, N1HAC, K4BSE, AF8A, W7LUX
and KB1HFT, respectively.

Competing interests. The authors declare that they have no conflict of interest.

Acknowledgements. We gratefully acknowledge the support of NSF Grants AGS-2002278, AGS-1932997, and AGS-1932972. This work
was undertaken through the HamSCI community (www.hamsci.org). We thank our volunteers for giving generously of their time and exper-
215 tise, particularly the maintainers of the first contingent of Grape stations for pioneering the PSWS network and the members of the WWV
Amateur Radio Club WW0WWV for their support with data curation. Hardware was constructed in the Sears Undergraduate Design Labo-
ratory and think[box] at CWRU, with support from the Case Amateur Radio Club W8EDU. Fast Light Digital Modem Application (fldigi) is
maintained by David Freese W1HKJ. We thank the developers of all python packages and open source software projects used in the analysis
code documented here. Finally, we thank the staff of WWV, WWVH and CHU, without whom this work would not be possible.

220 **References**

Atilaw, T. Y., Stephenson, J. A., and Katamzi-Joseph, Z. T.: Multitaper analysis of an MSTID event above Antarctica on 17 March 2013, Polar Science, 28, 100 643, https://doi.org/10.1016/j.polar.2021.100643, superDARN / Studies of Geospace Dynamics - Today and Future, 2021.

Benson, R. F.: Electron collision frequency in the ionospheric D region, Radio Science, 68D, 1123–1126, https://nvlpubs.nist.gov/nistpubs/
225   jres/68D/jresv68Dn10p1123_A1b.pdf, 1964.

Blagoveshchenskii, D. V.: Effect of geomagnetic storms (substorms) on the ionosphere: 1. A review, Geomagnetism and Aeronomy 2013 53:3, 53, 275–290, https://doi.org/10.1134/S0016793213030031, 2013.

Bristow, W., Greenwald, R., and Samson, J.: Identification of high-latitude acoustic gravity wave sources using the Goose Bay HF radar, Journal of Geophysical Research: Space Physics, 99, 319–331, 1994.

230 Buonsanto, M. J.: Ionospheric Storms — A Review, Space Science Reviews, 88, 563–601, https://doi.org/10.1023/A:1005107532631, 1999.

Chakraborty, S., Ruohoniemi, J. M., Baker, J. B. H., and Nishitani, N.: Characterization of Short-Wave Fadeout Seen in Daytime {Super-DARN} Ground Scatter Observations, Radio Science, 53, 472–484, https://doi.org/10.1002/2017RS006488, 2018.

Chakraborty, S., Ruohoniemi, J. M., Baker, J. B., Fiori, R. A., Bailey, S. M., and Zawdie, K. A.: Ionospheric Sluggishness: A Characteristic Time-Lag of the Ionospheric Response to Solar Flares, Journal of Geophysical Research: Space Physics, 126, e2020JA028 813,
235   https://doi.org/10.1029/2020JA028813, 2021.

Chilcote, M., LaBelle, J., Lind, F. D., Coster, A. J., Miller, E. S., Galkin, I. A., and Weatherwax, A. T.: Detection of traveling ionospheric disturbances by medium-frequency Doppler sounding using AM radio transmissions, Radio Science, 50, 249–263, https://doi.org/10.1002/2014RS005617, 2015.

Collins, K.: Grape Version 1, https://doi.org/10.17632/NBBHY2YXMZ.1, 2021.

240 Collins, K.: Grape V1 Data: Frequency Estimation and Amplitudes of North American Time Standard Stations, https://doi.org/10.5281/ZENODO.6584416, 2022.

Collins, K., Kazdan, D., and Frissell, N. A.: Ham Radio Forms a Planet-Sized Space Weather Sensor Network, Eos, 102, https://doi.org/10.1029/2021eo154389, 2021.

Collins, K., Cerwin, S., Erickson, P., Joshi, D., Frissell, N., and Huba, J.: Methods for Estimation of Ionospheric Layer Height
245   Characteristics from Doppler Frequency and Time of Flight Measurements on HF Skywave Signals, EGUsphere, 2022, 1–24, https://doi.org/10.5194/egusphere-2022-327, 2022a.

Collins, K., Montare, A., Frissell, N., and Kazdan, D.: Citizen Scientists Conduct Distributed Doppler Measurement for Ionospheric Remote Sensing, IEEE Geoscience and Remote Sensing Letters, 19, 1–5, https://doi.org/10.1109/lgrs.2021.3063361, 2022b.

Crowley, G. and Rodrigues, F. S.: Characteristics of traveling ionospheric disturbances observed by the TIDDBIT sounder, Radio Science,
250   47, https://doi.org/10.1029/2011RS004959, 2012.

Dellinger, J. H.: Sudden Disturbances of the Ionosphere, Proceedings of the Institute of Radio Engineers, 25, 1253–1290, https://doi.org/10.1109/JRPROC.1937.228657, 1937.

Frissell, N., Collins, K., Montare, A., and Benedict, R.: Plotting code for Grape V1 Doppler stations, https://doi.org/10.5281/zenodo.6654901, 2022a.

255 Frissell, N. A., Baker, J. B. H., Ruohoniemi, J. M., Gerrard, A. J., Miller, E. S., Marini, J. P., West, M. L., and Bristow, W. A.: Climatology
     of medium-scale traveling ionospheric disturbances observed by the midlatitude Blackstone SuperDARN radar, Journal of Geophysical
     Research: Space Physics, 119, https://doi.org/10.1002/2014JA019870, 2014.

     Frissell, N. A., Baker, J. B. H., Ruohoniemi, J. M., Greenwald, R. A., Gerrard, A. J., Miller, E. S., and West, M. L.: Sources and Characteristics
     of Medium Scale Traveling Ionospheric Disturbances Observed by High Frequency Radars in the North American Sector, Journal of
260 Geophysical Research: Space Physics, https://doi.org/10.1002/2015JA022168, 2016.

     Frissell, N. A., Kaeppler, S. R., Sanchez, D. F., Perry, G. W., Engelke, W. D., Erickson, P. J., Coster, A. J., Ruohoniemi, J. M., Baker,
     J. B., and West, M. L.: First Observations of Large Scale Traveling Ionospheric Disturbances Using Automated Amateur Radio Receiving
     Networks, Geophysical Research Letters, 49, e2022GL097 879, https://doi.org/10.1029/2022GL097879, 2022b.

     Galvan, D. A., Komjathy, A., Hickey, M. P., and Mannucci, A. J.: The 2009 Samoa and 2010 Chile tsunamis as observed in the ionosphere
265 using GPS total electron content, Journal of Geophysical Research: Space Physics, 116, n/a–n/a, https://doi.org/10.1029/2010JA016204,
     2011.

     Gao, J. S., Huth, A. G., Lescroart, M. D., and Gallant, J. L.: Pycortex: an interactive surface visualizer for fMRI, Frontiers in Neuroinformat-
     ics, 9, https://doi.org/10.3389/fninf.2015.00023, 2015.

     Georges, T. M.: HF Doppler studies of traveling ionospheric disturbances, Journal of Atmospheric and Terrestrial Physics, 30, 735–746,
270 https://doi.org/10.1016/S0021-9169(68)80029-7, 1968.

     Gibbons, J., Collins, K., Kazdan, D., and Frissell, N.: Grape Version 1: First prototype of the low-cost personal space weather station receiver,
     HardwareX, 11, e00 289, https://doi.org/10.1016/J.OHX.2022.E00289, 2022a.

     Gibbons, J., Collins, K., Kazdan, D., and Frissell, N.: Grape Version 1: First prototype of the low-cost personal space weather station receiver,
     HardwareX, 11, e00 289, https://doi.org/10.1016/j.ohx.2022.e00289, 2022b.

275 Gjerloev, J. W., Greenwald, R. A., Waters, C. L., Takahashi, K., Sibeck, D., Oksavik, K., Barnes, R., Baker, J., and Ruohoniemi,
     J. M.: Observations of Pi2 pulsations by the Wallops HF radar in association with substorm expansion, Geophys. Res. Lett., 34,
     https://doi.org/10.1029/2007GL030492, 2007.

     Grocott, A., Hosokawa, K., Ishida, T., Lester, M., Milan, S. E., Freeman, M. P., Sato, N., and Yukimatu, A. S.: Characteristics of medium-
     scale traveling ionospheric disturbances observed near the Antarctic Peninsula by HF radar, Journal of Geophysical Research: Space
280 Physics, https://doi.org/10.1002/jgra.50515, 2013.

     Hines, C. O.: Internal Atmospheric Gravity Waves at Ionospheric Heights, Canadian Journal of Physics, 38, 1441–1481,
     https://doi.org/10.1139/p60-150, 1960.

     Hori, T., Nishitani, N., Shepherd, S. G., Ruohoniemi, J. M., Connors, M., Teramoto, M., Nakano, S., Seki, K., Takahashi, N., Kasahara, S.,
     Yokota, S., Mitani, T., Takashima, T., Higashio, N., Matsuoka, A., Asamura, K., Kazama, Y., Wang, S. Y., Tam, S. W., Chang, T. F., Wang,
285 B. J., Miyoshi, Y., and Shinohara, I.: Substorm-Associated Ionospheric Flow Fluctuations During the 27 March 2017 Magnetic Storm:
     SuperDARN-Arase Conjunction, Geophysical Research Letters, 45, 9441–9449, https://doi.org/10.1029/2018GL079777, 2018.

     Huba, J. D., Drob, D. P., Wu, T.-W., and Makela, J. J.: Modeling the ionospheric impact of tsunami-driven gravity waves with SAMI3:
     Conjugate effects, Geophysical Research Letters, 42, 5719–5726, https://doi.org/10.1002/2015GL064871, 2015.

     Hunsucker, R. D.: Atmospheric gravity waves generated in the high-latitude ionosphere: A review, Reviews of Geophysics, 20, 293–315,
290 https://doi.org/10.1029/RG020i002p00293, 1982.

     Hunsucker, R. D.: Vertical Sounders — the Ionosonde, pp. 67–93, Springer Berlin Heidelberg, Berlin, Heidelberg,
     https://doi.org/10.1007/978-3-642-76257-4_3, 1991.

Inc., P. T.: Collaborative data science, https://plot.ly, 2015.

Kelley, M. C.: On the origin of mesoscale TIDs at midlatitudes, Annales Geophysicae, 29, 361–366, https://doi.org/10.5194/angeo-29-361-2011, 2011.

Lynn, K. J.: A technique for calculating ionospheric Doppler shifts from standard ionograms suitable for scientific, HF communication, and OTH radar applications, Radio Science, 44, https://doi.org/10.1029/2009RS004210, 2009.

Nicolls, M. J. and Heinselman, C. J.: Three-dimensional measurements of traveling ionospheric disturbances with the Poker Flat Incoherent Scatter Radar, Geophysical Research Letters, 34, n/a–n/a, https://doi.org/10.1029/2007GL031506, 2007.

Nishioka, M., Tsugawa, T., Kubota, M., and Ishii, M.: Concentric waves and short-period oscillations observed in the ionosphere after the 2013 Moore EF5 tornado, Geophysical Research Letters, 40, 5581–5586, https://doi.org/10.1002/2013GL057963, 2013.

Nishitani, N., Ruohoniemi, J. M., Lester, M., Baker, J. B. H., Koustov, A. V., Shepherd, S. G., Chisham, G., Hori, T., Thomas, E. G., Makarevich, R. A., Marchaudon, A., Ponomarenko, P., Wild, J. A., Milan, S. E., Bristow, W. A., Devlin, J., Miller, E., Greenwald, R. A., Ogawa, T., and Kikuchi, T.: Review of the accomplishments of mid-latitude Super Dual Auroral Radar Network (SuperDARN) HF radars, 6, https://doi.org/10.1186/s40645-019-0270-5, 2019.

Prölss, G. W.: Ionospheric Storms at Mid-Latitude: A Short Review, in: Midlatitude Ionospheric Dynamics and Disturbances, pp. 9–24, American Geophysical Union (AGU), https://doi.org/10.1029/181GM03, 2008.

Romanek, V., Frissell, N. A., Liles, W., Gibbons, J., and Collins, K. V.: HF Doppler Observations of Traveling Ionospheric Disturbances in a WWV Signal Received with a Network of Low Cost HamSCI Personal Space Weather Stations, in: HamSCI Workshop 2022, Huntsville, AL, https://hamsci.org/publications/hf-doppler-observations-traveling-ionospheric-disturbances-wwv-signal-received-3, 2022.

Samsel, F., Klaassen, S., and Rogers, D. H.: ColorMoves: Real-time Interactive Colormap Construction for Scientific Visualization, IEEE Computer Graphics and Applications, 38, 20–29, https://doi.org/10.1109/MCG.2018.011461525, 2018.

Scotto, C., Pezzopane, M., and Zolesi, B.: Estimating the vertical electron density profile from an ionogram: On the passage from true to virtual heights via the target function method, Radio Science, 47, https://doi.org/https://doi.org/10.1029/2011RS004833, 2012.

Thomas, E. G., Baker, J. B. H., Ruohoniemi, J. M., Coster, A. J., and Zhang, S.-R.: The geomagnetic storm time response of GPS total electron content in the North American sector, Journal of Geophysical Research: Space Physics, 121, 1744–1759, https://doi.org/10.1002/2015JA022182, 2016.

Trop, C.: Traveling Ionospheric Disturbances Tracked Through Doppler-Shifted AM Radio Transmissions, Dartmouth College Undergraduate Honors Thesis, https://physics.dartmouth.edu/events/event?event=63569, 2021.

Trop, C., LaBelle, J., Erickson, P. J., Zhang, S., McGaw, D., and Kovacs, T.: Traveling ionospheric disturbances tracked through Doppler-shifted AM radio transmissions, in: HamSCI Workshop 2021, HamSCI, Scranton, PA (Virtual), https://hamsci.org/publications/traveling-ionospheric-disturbances-tracked-through-doppler-shifted-am-radio, 2021.

Vierinen, J., Coster, A. J., Rideout, W. C., Erickson, P. J., and Norberg, J.: Statistical framework for estimating GNSS bias, Atmospheric Measurement Techniques, 9, 1303–1312, https://doi.org/10.5194/amt-9-1303-2016, 2016.

Zhang, S.-R., Erickson, P. J., Gasque, L. C., Aa, E., Rideout, W., Vierinen, J., Goncharenko, L. P., and Coster, A. J.: Electrified Postsunrise Ionospheric Perturbations at Millstone Hill, Geophysical Research Letters, 48, e2021GL095151, https://doi.org/10.1029/2021GL095151, 2021.